ISSN 1001-0742
CN 11-2629/X

JES JOURNAL OF ENVIRONMENTAL SCIENCES

December 1, 2014 Volume 26 Number 12
www.jesc.ac.cn

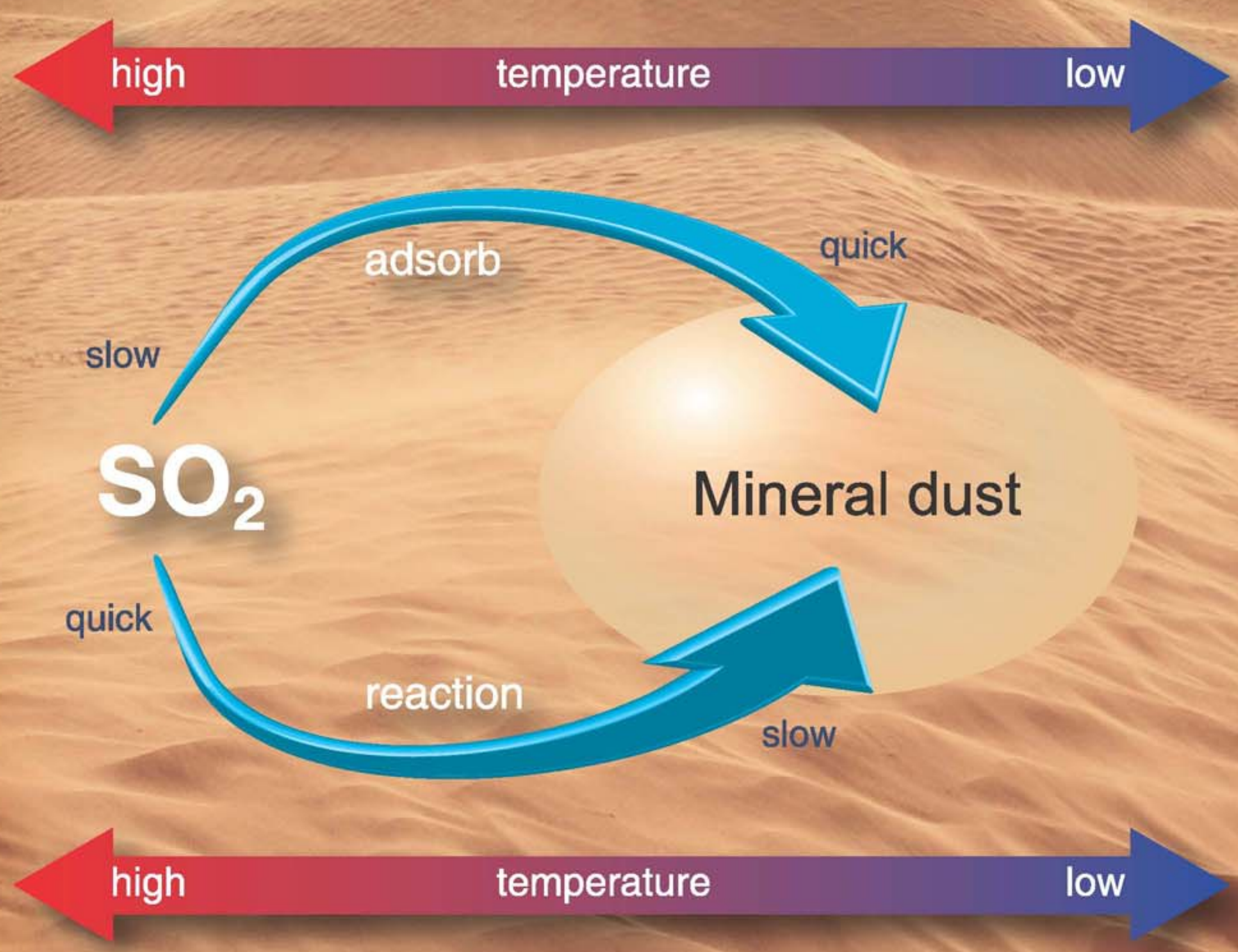

ELSEVIER
Science Press

Sponsored by
Research Center for Eco-Environmental Sciences
Chinese Academy of Sciences

Journal of Environmental Sciences Volume 26 Number 12 2014

www.jesc.ac.cn

CONTENTS

JOURNAL OF ENVIRONMENTAL SCIENCES 26 (2014) 2459–2474

Available online at www.sciencedirect.com

ScienceDirect

www.journals.elsevier.com/journal-of-environmental-sciences

Direct radiative forcing of urban aerosols over Pretoria (25.75°S, 28.28°E) using AERONET Sunphotometer data: First scientific results and environmental impact

Ayodele Joseph Adesina[1], *Kanike Raghavendra Kumar*[1,2,*], *Venkataraman Sivakumar*[1], *Derek Griffith*[3]

1. *Discipline of Physics, School of Chemistry and Physics, College of Agriculture, Engineering and Science, Westville Campus, University of KwaZulu–Natal, Durban 4000, South Africa*
2. *Key Laboratory for Aerosol-Cloud-Precipitation of China Meteorological Administration, School of Atmospheric Physics, Nanjing University of Information Science and Technology, Nanjing 210044, China*
3. *Optronic Sensor Systems, Council for Scientific and Industrial Research (CSIR)–DPSS, Pretoria 0001, South Africa*

ARTICLE INFO

Article history:
Received 8 January 2014
Revised 26 March 2014
Accepted 17 April 2014
Available online 22 October 2014

Keywords:
Pretoria
AERONET
Aerosol optical depth
Single scattering albedo
Radiative forcing

ABSTRACT

The present study uses the data collected from Cimel Sunphotometer of Aerosol Robotic Network (AERONET) for the period from January to December, 2012 over an urban site, Pretoria (PTR; 25.75°S, 28.28°E, 1449 m above sea level), South Africa. We found that monthly mean aerosol optical depth (AOD, τ_a) exhibits two maxima that occurred in summer (February) and winter (August) having values of 0.36 ± 0.19 and 0.25 ± 0.14, respectively, high-to-moderate values in spring and thereafter, decreases from autumn with a minima in early winter (June) 0.12 ± 0.07. The Angstrom exponents ($\alpha_{440-870}$) likewise, have its peak in summer (January) 1.70 ± 0.21 and lowest in early winter (June) 1.38 ± 0.26, while the columnar water vapor (CWV) followed AOD pattern with high values (summer) at the beginning of the year (February, 2.10 ± 0.37 cm) and low values (winter) in the middle of the year (July, 0.66 ± 0.21 cm). The volume size distribution (VSD) in the fine-mode is higher in the summer and spring seasons, whereas in the coarse mode the VSD is higher in the winter and lower in the summer due to the hygroscopic growth of aerosol particles. The single scattering albedo (SSA) ranged from 0.85 to 0.96 at 440 nm over PTR for the entire study period. The averaged aerosol radiative forcing (ARF) computed using SBDART model at the top of the atmosphere (TOA) was −8.78 ± 3.1 W/m^2, while at the surface it was −25.69 ± 8.1 W/m^2 leading to an atmospheric forcing of +16.91 ± 6.8 W/m^2, indicating significant heating of the atmosphere with a mean of 0.47 K/day.

Introduction

Tropospheric aerosols, also known as particulate matter (PM), are produced by both natural and anthropogenic processes. Natural sources include windblown mineral dust, precursor gases from volcanic eruptions, natural wild fires, vegetation and oceans. Anthropogenic sources include emissions from fossil fuel and bio fuel combustions, industrial processes, agricultural practices, human induced biomass burning and photochemically induced smog primarily, due to vehicle emissions (Levy et al., 2007; Tesfaye et al., 2011). Unlike greenhouse gases (GHGs), tropospheric aerosols have short life time (about few weeks or less), and

* *Corresponding author*. E-mail: krkumar@nuist.edu.cn (Kanike Raghavendra Kumar).

http://dx.doi.org/10.1016/j.jes.2014.04.006

therefore, their spatial distribution is highly inhomogeneous and strongly correlated with their sources. Also, they vary in size by orders of magnitude and their properties change as they interact within the atmosphere (Rajeev et al., 2000). They are being removed by clouds and dry deposition processes. Despite relatively short average residence times, they travel long distances.

Atmospheric aerosols, derived from natural as well as anthropogenic emission sources, are important and significantly contribute to Earth's radiation budget through a variety of pathways such as direct effects on scattering and absorption of solar radiation, indirect effects on cloud microphysics, and semi-direct effects (Kaufman et al., 2002; Yoon et al., 2005; Ramanathan et al., 2007; Ramanathan and Carmichael, 2008; Kim et al., 2010). These aerosols are known to affect the air quality, human health and radiation budget, and understanding their climatic and environmental effects has been a central theme for the global scientific community. Most of the aerosol particles such as sulfate and sea salt, mainly scatter solar radiation, while black carbon aerosols strongly absorb radiation (Ramanathan and Carmichael, 2008). Regardless of whether the aerosol absorbs or scatters radiation, less solar radiation penetrates to the Earth's surface (Lohmann et al., 2010). Furthermore, such effects are determined by their optical, physical, radiative and chemical characteristics in concert with source, strength and/or advection by local synoptic meteorological processes.

The direct radiative effect (DRE) due to aerosols is defined as the effect of total aerosols (both natural and anthropogenic) on the radiative fluxes primarily due to the direct scattering and absorption of solar radiation by aerosols and is measured in terms of watts per square meter termed as aerosol direct radiative forcing (ADRF or simply ARF) (Chung et al., 2005; Srivastava et al., 2012). The values of radiative forcing (RF) at the bottom (RF_{BOA}) and top (RF_{TOA}) of the atmosphere are key parameters in the quantification of the impact of aerosols on climate. The ARF due to aerosols is one of the largest sources of uncertainties in estimating climate perturbations due to large spatial variability of aerosols and the lack of an adequate database on their radiative properties (IPCC, 2007). Some estimates suggest that anthropogenic aerosols and biomass burning have climate forcing enough to offset warming caused by GHGs such as carbon dioxide (Kiehl and Briegle, 1993).

According to the Intergovernmental Panel on Climate Change (IPCC, 2001) Fourth Assessment Report, the global average radiative forcing by aerosols is -1.2 W/m^2, whereas, it is about 2.6 W/m^2 for GHGs. Much attention has been paid to quantifying the radiative forcing by aerosols (Pandithurai et al., 2008). Therefore, measuring and understanding changes in aerosol loading over time are highly essential to predict climate change (Tesfaye et al., 2011). For this purpose, different ground- and satellite-based remote sensing techniques are providing a systematic retrieval of aerosol optical properties on the global and regional scale (Kaufman et al., 2002; Kahn et al., 2010; More et al., 2013; Alam et al., 2014). Satellite data does not provide a complete characterization of the optical properties of aerosols, or information on their other characteristics (Eck et al., 2005). A major advance in this respect has been the introduction of the Aerosol Robotic Network (AERONET) (Holben et al., 1998), which means that satellite remote sensing of aerosols no longer needs to be largely independent but can be tied in to this coordinated and harmonised ground data network. Ground-based remote sensing has become a powerful method for characterizing atmospheric aerosols (Dubovik and King, 2000) as it is able to present a clear picture of the optical properties of each of the aerosol species (Dubovik et al., 2002; Cattrall et al., 2005).

South Africa is a developing country and lies in the extreme bottom of southern part of African continent. It has four distinct seasons; summer (December–February; DJF), autumn (March–May; MAM), winter (June–August; JJA) and spring (September–November; SON). Aerosol radiative forcing (ARF) and optical properties have not been studied in the Pretoria (PTR; 25.75°S, 28.28°E, 1449 m above sea level) (Fig. 1) region where atmospheric brown clouds (ABCs) are frequently observed (Ramanathan and Carmichael, 2008) with large amount of absorbing aerosols emitted due to biomass burning and/or forest fires which includes black carbon (Queface et al., 2011). In this study, the previously reported work by Kumar et al. (2013a) has been expanded to give detailed description of aerosol optical, microphysical and radiative properties for the first time over PTR, an urban site in the northwest part of South Africa.

The data from the AERONET Sunphotometer over PTR for one year period of 2012 has been used in the present work to study the significant changes in the aerosol properties. Here we examined the aerosol optical, microphysical and radiative properties in terms of aerosol optical depth (AOD), Ångström wavelength exponent ($\alpha_{440-870}$), particle volume size distribution, single scattering albedo (SSA), and asymmetry parameter (ASP), together with the real (Re) and imaginary (Im) parts of the complex refractive index (RI). Airmass trajectories (7-day back-trajectory) have been used to trace the source, path and spatial extent of mineral dust and smoke events using National Oceanic and Atmospheric Administration (NOAA) Hybrid Single-Particle Lagrangian Integrated Trajectory (HYSPLIT) model. Further, the monthly average ARF and forcing efficiencies were calculated using the Santa Barbara DISORT Atmospheric Radiative Transfer (SBDART) model (Ricchiazzi et al., 1998), and compared with the magnitudes derived from AERONET to know the impact on environment and climate change.

1. Experimental site, instrumentation and methods

1.1. Site description

An automatic sun/sky radiometer (Cimel Electronique, Paris, France) was set up at PTR operational since July 2011 under the joint collaboration between NASA and the Pretoria's office of Council for Scientific and Industrial Research (CSIR). PTR is one of the three capital cities of the nation, serving as the administrative capital. It is situated in a transitional belt between the plateau of the Highveld to the south and the lower lying Bushveld to the north approximately 55 km northeast of Johannesburg city in South Africa. The city has a humid subtropical climate with long hot and rainy summers, and short cool and dry winters. The major industries in PTR include the manufacture of motorcycles, chemicals, pharmaceuticals, engineering products, construction materials, steel industries, oil refineries, cement factories, and power plants. In addition to the industrial emissions, other anthropogenic sources that include vehicular emissions from main highways, coal combustion, agricultural and biomasses burning are the major local sources of aerosol in this capital city of South Africa. The aerosols derive mainly from soil or road dust, sea-salt particles from the Indian Ocean and secondary aerosols produced from biomass burning.

1.2. Measurements

Sun/sky radiometer (Model: CE318, Cimel Electronique, Paris, France), which is placed on the roof of a building to make free from tall buildings and trees, takes measurements of the direct beam and sun/sky almucantar radiance measurements provide column-integrated spectral aerosol optical depths (AODs) from 340 to 1020 nm and 440–1020 nm, respectively (Holben et al., 1998). Seven of the eight bands are used to

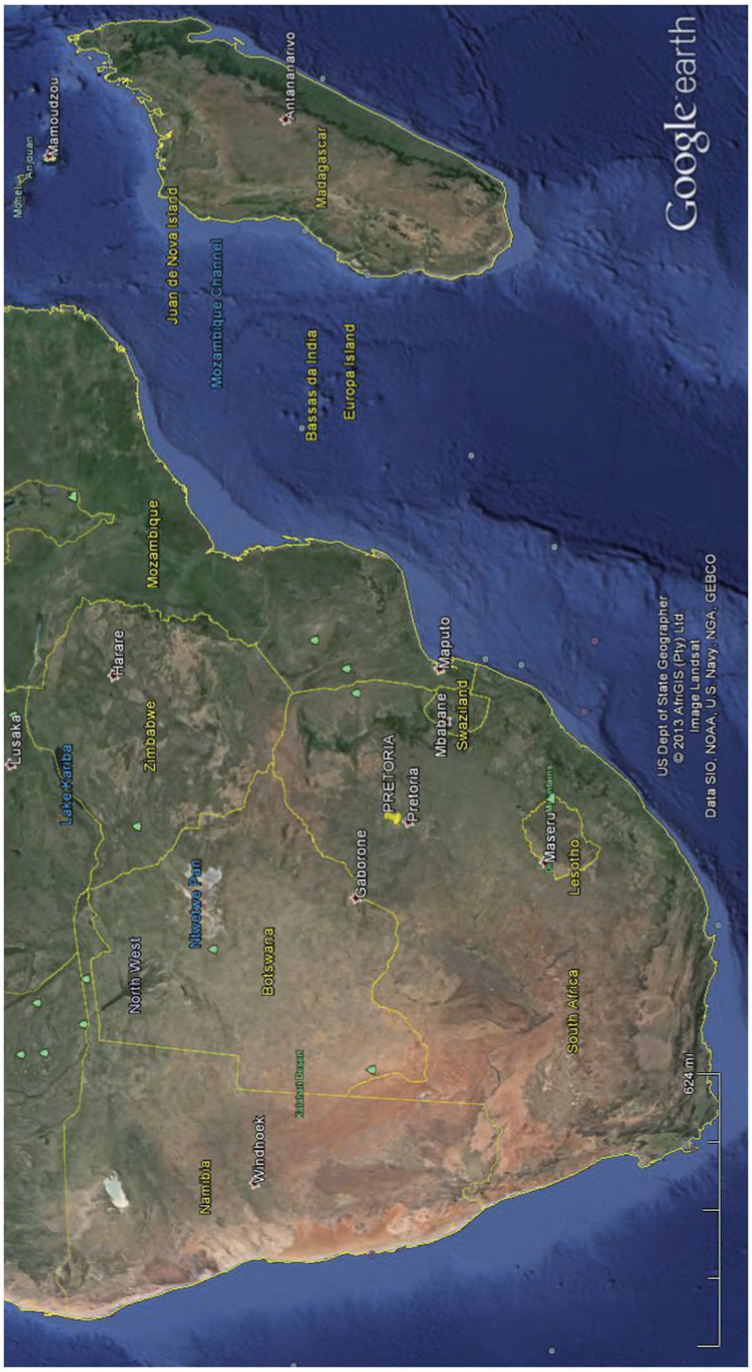

Fig. 1 – Satellite map showing the region of study (Pretoria) in South Africa denoted with a yellow color needle pointer and other surrounding areas. Source: Google Earth Maps.

acquire AOD data, while the eight band 940 nm is used to estimate total columnar water vapor (CWV) in the atmosphere. A careful assessment of the overall uncertainty in computed AOD due to calibration uncertainty typically for a field instrument is ±0.01 to ±0.02 which is spectral dependent with higher errors in the UV spectral range (Eck et al., 1999; Smirnov et al., 2002). Furthermore, from the almucantar measurements and the spectral deconvolution algorithm (SDA) retrievals, aerosol volume size distribution (VSD), single scattering albedo (SSA), asymmetry parameter (ASP), refractive index (RI), fine- and coarse-mode AODs are also available for large solar zenith angles (>50°) and high aerosol loading conditions (AOD440 > 0.4) (Dubovik et al., 2000). More details about the instrument, uncertainties, error estimation *etc*., are discussed by several earlier researchers (Holben et al., 1998; Eck et al., 1999; Dubovik et al., 2002). The data of PTR station are obtained from the AERONET website (http://aeronet.gsfc.nasa.gov/) and version 2.0/level 2.0 of the quality assured daily points' format data of direct sun and inversion products are used for the study period of January–December, 2012.

1.3. Methods to obtain AOD and inversion products

The effect of radiative transfer is proportional to the amount of particles present in the column but it also depends on their intrinsic optical properties. The spectral variation of AOD provides useful information on columnar size distribution and can be best represented by Ångström power law relationship, given by Ångström (1964):

$$\tau_a(\lambda) = \beta\lambda^{-\alpha} \tag{1}$$

where, τ_a (λ) is the AOD at wavelength λ (in micrometers), β is the turbidity coefficient, indicating total aerosol loading, which equals to τ_a at λ = 1 μm, and α is widely known as the Ångström exponent (AE), which is a good indicator of aerosol particle size (Eck et al., 1999). AE largely depends on aerosol size distribution and is a measure of the ratio of coarse- to fine-mode aerosols, with higher values representing increased abundance of fine-mode aerosols and lower values representing increased abundance of coarse-mode aerosols (Kumar et al., 2009; Srivastava et al., 2012).

Besides the information contained directly in the AOD and its spectral dependence, an inversion algorithm developed by Dubovik and King (2000) and subsequently modified by Dubovik et al. (2002) can be used to retrieve the columnar aerosol's characteristics from the direct sun and diffuse sky radiance measurements. In the most recent version (Version 2.0) of the inversion algorithm (Dubovik et al., 2006), the vertically averaged aerosol volume size distribution (dV/dlnrin a range of radii between 0.05 and 15 μm, the real and imaginary parts of the aerosol complex refractive index, the scattering phase function, which in turn allows computation of the asymmetry parameter (*g*), and the single scattering albedo (SSA) are retrieved in the inversion data products of AERONET data. The above last two quantities are crucial inputs for the radiative transfer codes used for the quantification of the aerosol's impact on radiative transfer. Another important addition in the Version 2.0 inversion products is that a new set of radiative properties is given at any AERONET station. More details and computations of these parameters were described elsewhere by many researchers to name a few, El-Metwally et al. (2011) and Esteve et al. (2014) in their respective works.

1.4. HYSPLIT trajectory model

The HYSPLIT_4 (http://www.arl.noaa.gov; Air Resources Laboratory, National Oceanic and Atmospheric Administration, USA) model is a system with simple graphical user interface for computing trajectories and air concentrations (Draxler and Hess, 1998). Gridded meteorological data at regular time intervals are used in the calculation of airmass trajectories. For back-trajectories, data are obtained from existing archives. A complete description of input data, methodology, equations involved, and sources of error for calculation of airmass trajectory can be found in Draxler and Hess (1998). The model is run directly on the web (http://www.arl.noaa.gov/ready/hysp_info.html) by giving necessary inputs or on local PC after installing the software and input data set. The executables and meteorological data are provided by the NOAA ARL (Air Resources Laboratory) for free for back-trajectory analysis and registration is required for forecast analysis. The model gives output in the form of post-script image and as well as ASCII form that can be imported in other programs for plotting.

2. Results and discussion

2.1. Synoptic meteorological conditions

The monthly mean variations of prevailing background meteorological conditions over the site (PTR) during the study period are shown in Fig. 2a–c. The data was provided by South African Weather Service (SAWS) from the surface at an altitude of 1449 m above sea level during the study period. The total annual rainfall recorded for the study period stands at 573.4 mm (Fig. 2a). The station experienced high wind speed during the spring and summer and low during the autumn and winter. The maximum value was recorded in the September of 1.6 ± 0.6 m/sec and minimum in the month of May, which is 0.5 ± 0.2 m/sec (Fig. 2b). The direction of wind is generally from the south, apart from July–August where it is from the southeast. Ambient air temperature is the lowest in June during the winter and keeps on increasing till November. It goes down a little in December and January and rose to another peak in February and thereafter, it decreases till June. The maximum air temperature at the two maxima was noticed to be 30.3°C in February and November, while the minimum of 5.5°C was recorded in June (not shown in figure). The average monthly temperature was observed high in February with a value of 24.9 ± 1.2°C and low value of 12.8 ± 2.0°C in June (see Fig. 2c). Relative humidity ranges from 36% in August to 63% in December due to an increase in diurnal temperatures (Fig. 2c). It fairly decreases from January to August and begins to rise till December.

2.2. Variabilities in aerosol optical properties

The aerosol optical depth is representative of the airborne aerosol loading in the atmospheric column, and is important for the identification of aerosol source regions and aerosol evolution. Fig. 3a–c illustrates the monthly averaged AOD_{500}, CWV and $\alpha_{440-870}$ for twelve months (January–December 2012) in PTR with the standard deviation. A total of 333 daily averages contributed to the statistics to represent the figures. It can be easily found that AOD showed a distinct seasonal variation in this urban area with high values that mainly occurred in summer. Two maxima of AOD_{500} were recorded during the year in February (summer) and August (early of spring or late winter) with values of 0.36 ± 0.19 and 0.25 ± 0.14, respectively, while the minimum was observed in April/June (late autumn or winter) which is of 0.12 ± 0.07 (Fig. 3a). The appearance of high values of AOD_{500} in summer was related to high convective activity and contribution of dust and smoke particles emitted from surrounding regions by the long-range transport, which is clearly evident from HYSPLIT model described in the following paragraphs (Fig. 4a–d).

The occurrence of high value in urban region was also related to the anthropogenic pollution and local prevailing meteorological conditions. The high temperatures during January/February play an important role in heating ground and lifting the loose soil particles with association of wind speed (Devara et al., 2005; Yu et al., 2009; Kumar et al., 2009). Sometimes, the very high values of AOD_{500} (>0.5) noticed in the present study may possibly due to the presence of optically thin high altitude clouds over the experimental site. Further, higher AOD values particularly during the late winter months are considered to be due to combination of large-scale circulation processes and elevated temperature inversion-caused haze layer formations (Devara et al., 2005).

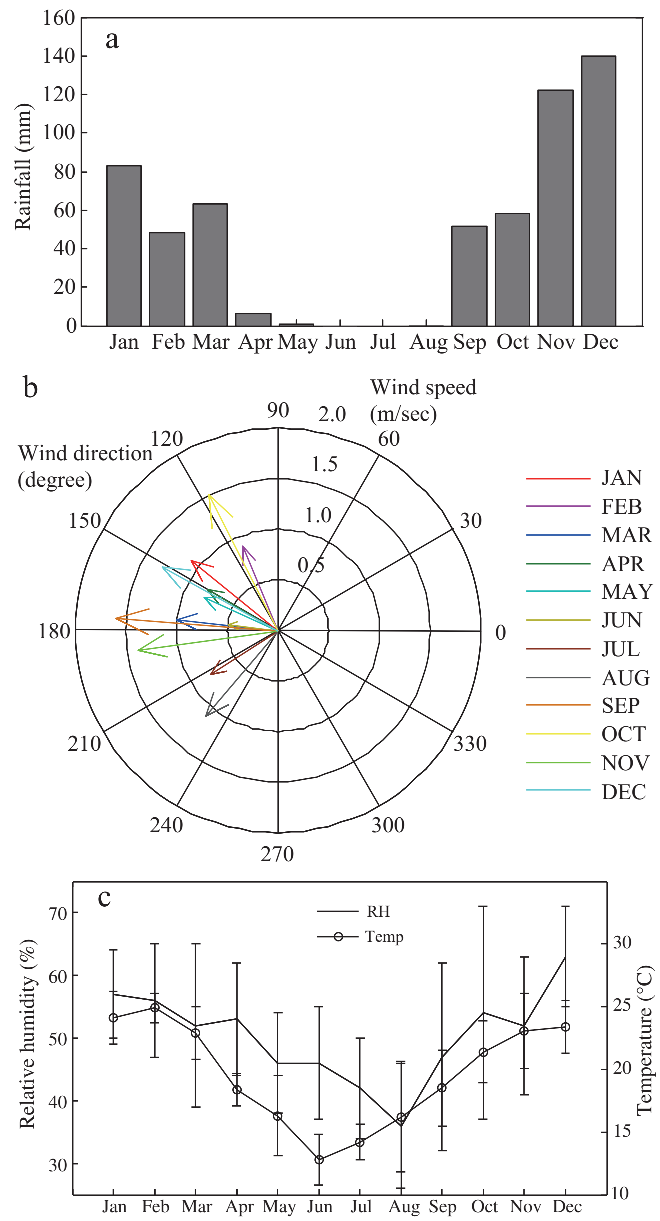

Fig. 2 – Monthly mean variations in (a) total annual rainfall, (b) polar chart representing wind speed and direction, and (c) average values of relative humidity and air temperature during the study period January–December, 2012 prevailing over Pretoria. Source: SAWS.

The decrease in AOD values has been observed during June compared to May because of dispersal of aerosol due to stronger wind speeds (see Fig. 2b), cloud-scavenging and rain-washout processes (Kumar et al., 2009).

In order to understand the origin of airmasses arriving in the studied region, we performed 7-day back-trajectory analyses based on the NOAA HYSPLIT model (Draxler and Rolph, 2003) with the GDAS as the meteorological input for the trajectory model. These trajectories are computed at three different levels 500 m, 1500 m and 3000 m above sea level. Fig. 4 represents 168 hr back-trajectories ending at observation site for typical days on 19th February, 10th April, 7th June and 7th October during four different seasons for the period of study. These trajectories are considered to be representative of the entire time period analyzed. Fig. 4a and d obtained on high AOD days during which the airmass parcels coming from the mainland of South Africa and surrounding arid/semi-arid regions traveling a short distance before reaching the measuring site. Fig. 4b, c indicates low AOD days where the trajectory at different levels has a long history originating from the pristine marine environment. These trajectories transport sea-salt (coarse) particles that get settled down before reaching the site due to their smaller residence times. Fig. 4d is obtained to show evidence of long-range transport of smoke particles emitted from biomass burning and/or forest fires traversing through Mozambique and Madagascar which occur every year during the spring season.

The CWV followed a pattern with high values in January (2.08 ± 0.32 cm) and February (2.10 ± 0.38 cm) followed by a decrease until June (0.68 ± 0.34 cm), July (0.66 ± 0.22 cm) and then an increase until December (2.00 ± 0.24 cm) (see Fig. 3b). The high (low) value of CWV which was noticed in February (July) corresponds to the high (low) aerosol loadings (AOD_{500}) which shows that AOD and CWV follow similar seasonal trend throughout the year. The correlation coefficient between CWV and AOD were found to be 0.41, which clearly suggests that aerosol particles over PTR are more hygroscopic and is consistent with the general synoptic pattern over the region. Ångström exponent (α) was a measure of the wavelength dependence of AOD and a good indicator of aerosol particle-size. It is clearly depicted from Fig. 3c that the monthly mean values of $\alpha_{440–870}$ were always greater than 1.5 throughout the year with more or less similar values in all months/seasons, except in the winter. These results signify the presence of greater contribution of aerosols in the fine-mode to the extinction for the present study period. The values range from 1.30 ± 0.26 in June to 1.70 ± 0.20 in January. The high values of both $\alpha_{440–870}$ and AOD_{500} which occurred in summer indicated that there was an increase in the contribution of fine-mode particles during the high temperature period (Lyamani et al., 2006).

In terms of seasonal variations, AOD_{500} has its peak value of 0.24 ± 0.16 in summer, followed by 0.20 ± 0.12 in spring, 0.18 ± 0.10 in winter and a low value of 0.16 ± 0.09 in autumn. This is unlike Skukuza (South Africa) or Mongu (Zambia) where the highest AOD_{500} occurred during the spring (biomass burning) season (Queface et al., 2011; Kumar et al., 2013b). We pointed out in our earlier study that this occurrence in summer in PTR can be attributed to the contribution of pollutant particles emitted from local anthropogenic sources and prevailing meteorological conditions, such as high temperature and the growth of hygroscopic particle with the increase in CWV during this period (Kumar et al., 2013a). The high value of 2.06 ± 0.32 cm for CWV was observed in summer, followed by 1.40 ± 0.50 cm in spring, 1.25 ± 0.42 cm in autumn and 0.69 ± 0.31 cm in winter. The $\alpha_{440–870}$ likewise, has its peak value of 1.67 ± 0.23 in summer, followed by 1.60 ± 0.23 in autumn, 1.52 ± 0.22 in spring and 1.41 ± 0.25 in winter.

The scatter plot of daily $\alpha_{440–870}$ *versus* AOD_{500} was shown in Fig. 5a; this allows one to define physically interpretable cluster regions for different types of aerosols or qualitative indication on aerosol load due to particles of different sizes (Smirnov et al., 2002; Bi et al., 2011; Sumit Kumar et al., 2011; Kumar et al., 2013b). For $AOD_{500} < 0.4$, the $\alpha_{440–870}$ values ranges between 0.8 and 1.2, a case of a mixture of both fine mode and coarse mode aerosols with dominance of fine mode aerosols. CWV and AOD_{500} shows a poor correlation ($R^2 = 0.41$) (Fig. 5b). For

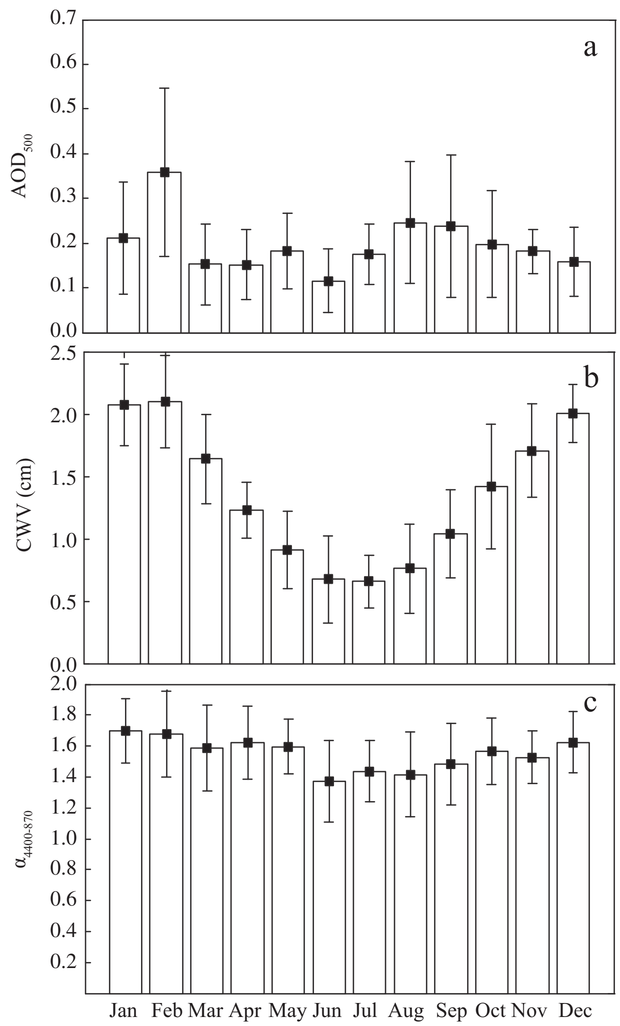

Fig. 3 – Monthly average (a) aerosol optical depth (AOD) at 500 nm, (b) columnar water vapor (CWV), and (c) Ångstrom exponent ($\alpha_{440–870}$) measured from Cimel Sunphotometer over Pretoria. The solid rectangular dot represents the mean and the vertical bars indicate the standard deviations of the mean.

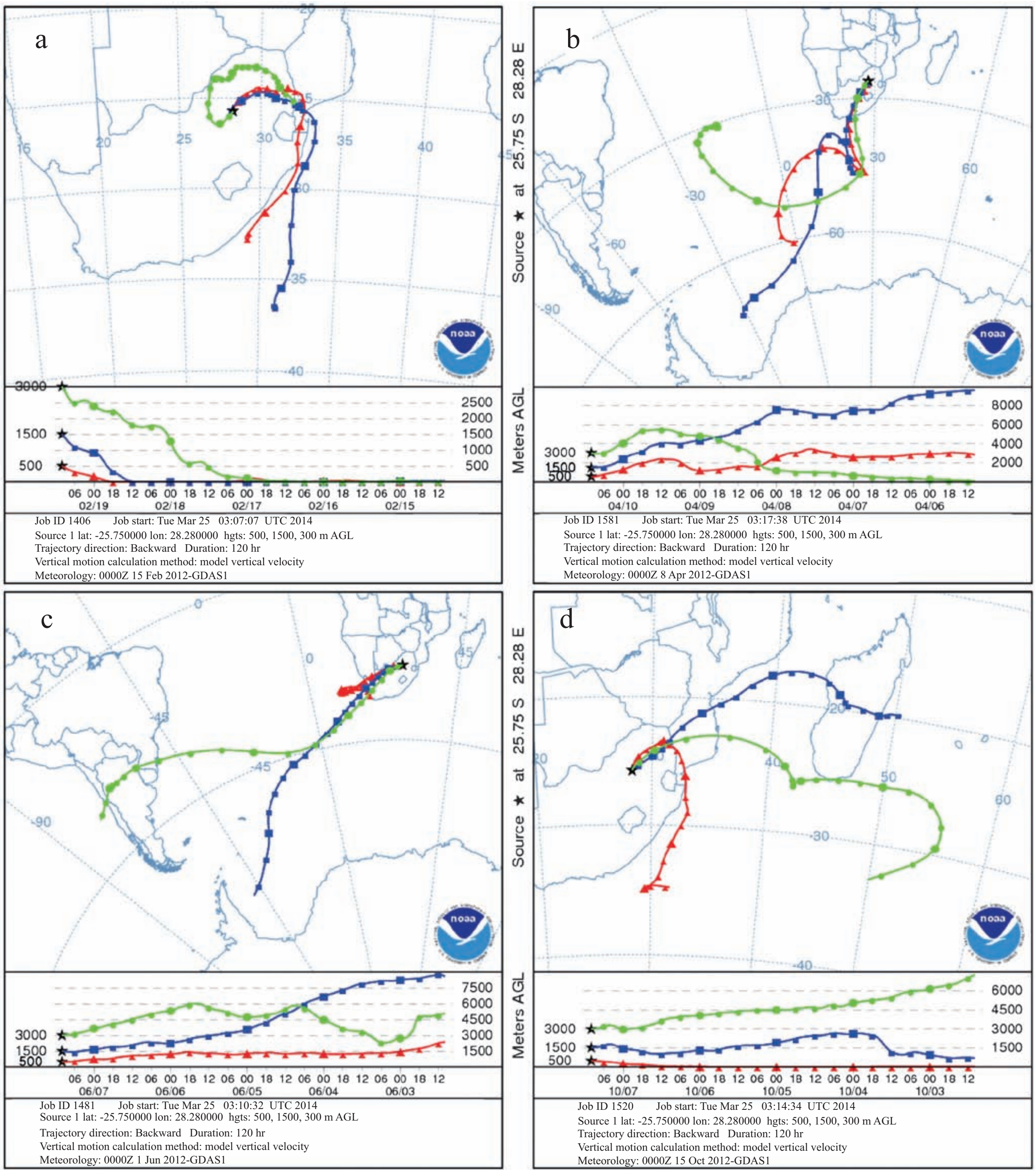

Fig. 4 – NOAA-HYSPLIT model run five-day backward trajectory analysis of airmass pathways at 500, 1500 and 3000 m altitudes on typical representative days during high AOD (a, d) and low AOD (b, c) in four different seasons over Pretoria.

AOD < 0.4, CWV ranges from 0.25 to 2.5. This may be the fact that aerosol and water vapor were being transported at different heights. Scatter plot of CWV and $\alpha_{440–870}$ which is showed in Fig. 5c has a significant correlation with coefficient of 0.55 as hygroscopic effect tends to make aerosol increase in their size.

Fig. 6 is the AOD_{500}, CWV and $\alpha_{440–870}$ showing the percentage of occurrences categorized by individual seasons. The autumn has the narrowest probability distribution with a modal value of 0.1 followed by the winter with same modal value. However, summer has the widest distribution with a modal value of 0.1 and spring has the modal value of 0.2. The highest seasonal value recorded is due to the fact that AOD_{500} of 0.2 and 0.3 values is quite appreciable forming over 40%. For $\alpha_{440–870}$, apart from summer when the modal was 1.8, the

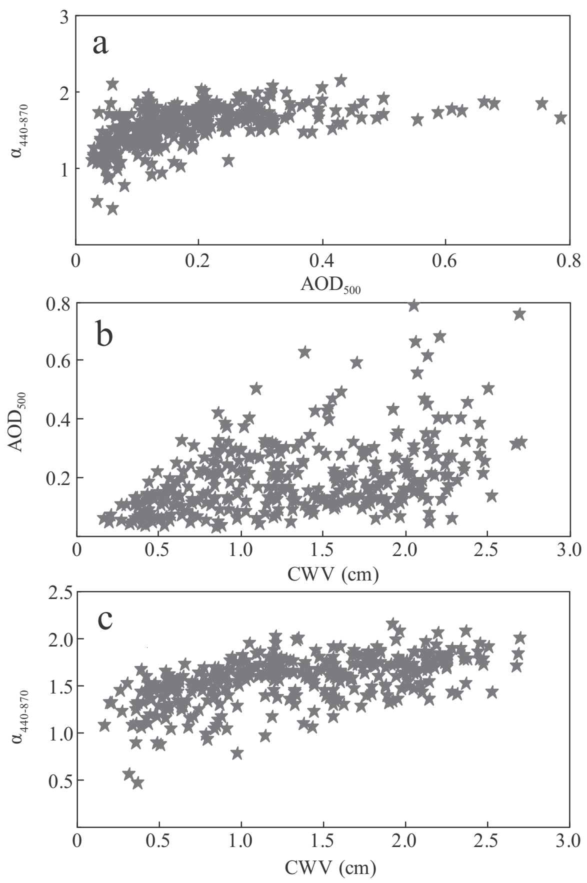

Fig. 5 – Scatter plots between different aerosol optical parameters during the study period over Pretoria.

modal value remained at 1.6 in all the seasons. The columnar water vapor ranges from 1.0–3.0 cm for summer with a modal value of 2.1 cm. The autumn and spring showed a wide distribution from 0.4–2.4 cm with a modal value of 1.2 cm, while in the winter, the range of distribution is from 0.2 to 1.5 cm with a modal of 0.5 cm.

2.3. Aerosol volume size distribution

The iterative inversion algorithm for retrieval of aerosol optical and microphysical properties including VSD, SSA, real (Re) and imaginary (Im) parts of refractive indices and asymmetry parameter (ASP) from sun and sky radiance data is contained in the work of Dubovik and King (2000). The inversion algorithm produces retrievals, which correspond to the effective optical properties for the total atmospheric column. In the retrieval algorithm, the aerosol particles are assumed to be poly-dispersed homogenous spheres (Smirnov et al., 2002). Dubovik et al. (2000) showed that the size distribution, in the case of nonspherical dust aerosols, can be retrieved reasonably well when the angular range of sky radiances is limited to angles smaller than 30°–40°. However, in order to retrieve the SSA the sky radiances acquired in the whole almucantar are needed along with the direct sun measurements. Thus for nonspherical dust aerosols, we should use the early morning or late afternoon (scattering angle range is large) sky radiance measurements to retrieve a single scattering albedo and sky radiances acquired around midday (scattering angle is small) to extract aerosol size distributions (Smirnov et al., 2002).

The aerosol VSD is an important parameter, which has an intense effect on climate. The worldwide aerosol size distribution exhibits two distinct modes: fine particles with particle size < 0.6 μm and coarse with particle size > 0.6 μm (Dubovik et al., 2002). In the present study, the AERONET VSDs ($dV(r)/d\ln r$) are retrieved from spectral and sun radiance data using the Dubovik and King (2000) approach, with the following initial guess: $dV(r)/d\ln r = 0.0001$, $n(\lambda_i) = 1.50$, $k(\lambda_i) = 0.005$, where $dV/d\ln r$ denotes aerosol volume size distribution, and $n(\lambda_i)$ and $k(\lambda_i)$ denote real and imaginary parts of the complex refractive index at a wavelength λ_i. The AERONET aerosol size distributions are retrieved from the Sunphotometer using 22 radius size bins in the size range of 0.05–15 μm. The volume size distributions exhibit a bimodal structure, which can be characterized by the sum of two log-normal distributions as follows:

$$\frac{dV(r)}{d\ln r} = \sum_{i=1}^{2} \frac{C_{V,i}}{\sqrt{2\pi}\sigma_i} \exp\left[-\frac{(\ln r - \ln r_{V,i})^2}{2\sigma_i^2}\right] \tag{2}$$

where, σ_i is the standard deviation, $r_{v,i}$ is the volume median radius and $C_{v,i}$ is the volume concentration for fine and coarse modes. More information about the calculation of different quantities involved in the above Eq. (2) was described by Alam et al. (2011).

Table 1 shows the parameters of the bimodal lognormal volume size distribution which reflects the monthly mean of each parameter. The volume geometric mean radius for fine aerosol was stable at 0.15 μm throughout the autumn. This size ranges between 0.14 and 0.15 μm in the winter and spring but goes higher in the summer ranging from 0.16 μm in December and January to 0.18 μm in February. The geometric mean radius for coarse mode aerosol was the lowest in December (3.02 μm) and the highest in June (3.27 μm) corresponding to the lowest value of $\alpha_{440–870}$. The volume concentration for fine aerosol doubled between January and February; whereas in the coarse, the volume concentration in August and September is nearly double than in January. The variations in VSD over PTR were mainly attributed due to the changes in the concentration of aerosol fine mode fraction with coefficient of variation (COV), defined as standard deviation to the mean, equal to 74%. The annual average fine and coarse mode particles geometric mean radii were 0.15 ± 0.02 and 3.17 ± 0.26, respectively. The COV yielded 14% for the fine mode R_f and 10% for σ_f, while 8% and 6% for the coarse mode and σ_f, respectively.

The seasonal average VSD ($dV(r)/d\ln r$) as shown in Fig. 7 represents a bimodal lognormal distribution with fine mode dominating at a radius of about 0.15 μm, whereas the coarse-mode is dominant with a radius of about 4 μm. The VSDs in the fine-mode are higher in the spring season than in the summer season and lower in the autumn season. The higher values in spring are due to the frequent biomass burning activities and forest fire events, whereas in the summer season it is due to the transport of mineral dust over this region and also due to meteorological conditions,

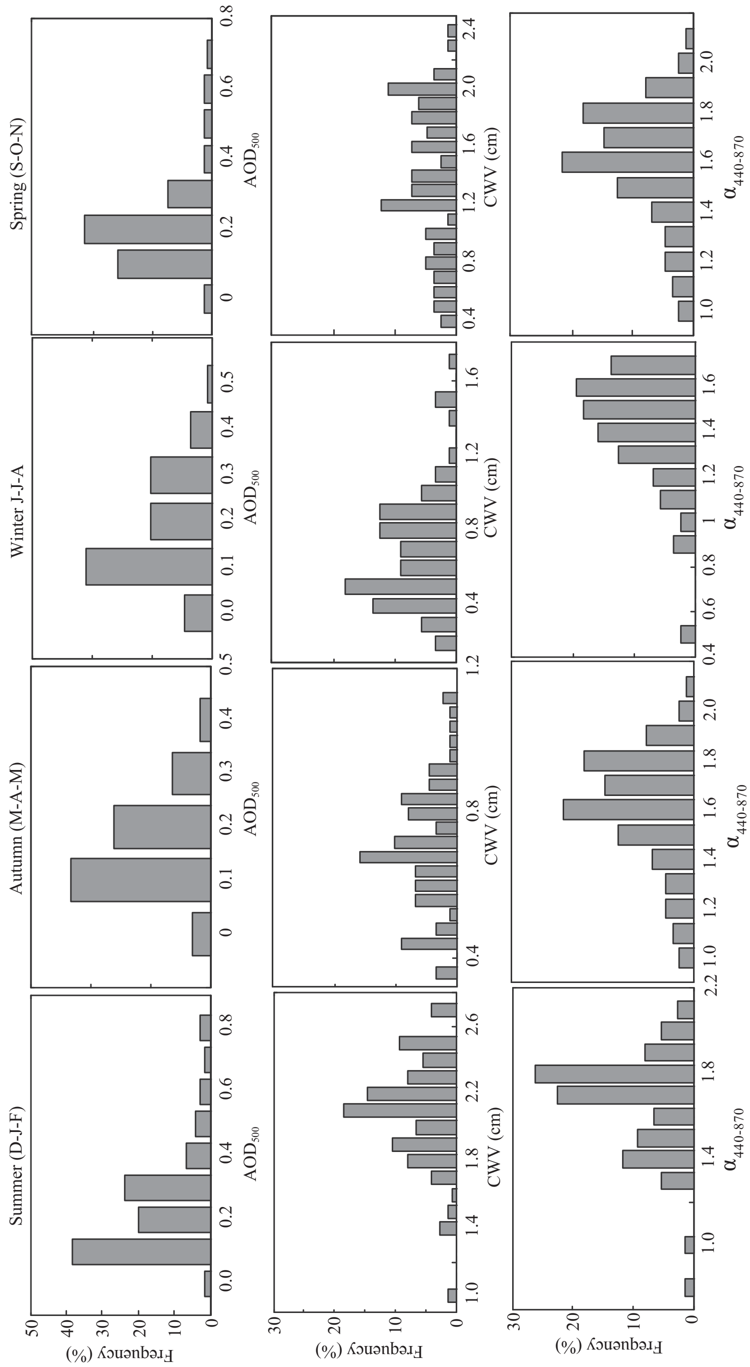

Fig. 6 – Seasonal frequency (%) distribution of AOD_{500}, CWV and $\alpha_{440-870}$.

Table 1 – Mean monthly of derived parameters from aerosol volume size distribution over Pretoria for 2012.

Month	Fine-mode				Coarse-mode			
	V_f	$R_{eff\ (f)}$	R_f	σ_f	V_c	$R_{eff\ (c)}$	R_c	σ_c
Jan-12	0.032	0.15	0.16	0.43	0.024	2.41	3.06	0.68
Feb-12	0.063	0.16	0.18	0.45	0.039	2.58	3.18	0.64
Mar-12	0.029	0.13	0.15	0.42	0.031	2.54	3.23	0.66
Apr-12	0.028	0.14	0.15	0.42	0.027	2.52	3.18	0.66
May-12	0.031	0.14	0.15	0.41	0.038	2.50	3.17	0.66
Jun-12	0.015	0.13	0.14	0.44	0.033	2.57	3.27	0.65
Jul-12	0.026	0.13	0.14	0.41	0.046	2.52	3.22	0.66
Aug-12	0.036	0.14	0.15	0.41	0.046	2.47	3.17	0.67
Sep-12	0.031	0.14	0.15	0.43	0.042	2.43	3.13	0.68
Oct-12	0.040	0.13	0.14	0.41	0.031	2.43	3.16	0.69
Nov-12	0.039	0.13	0.14	0.41	0.039	2.44	3.14	0.68
Dec-12	0.025	0.15	0.16	0.46	0.021	2.38	3.02	0.67
Mean	0.032	0.14	0.15	0.43	0.036	2.49	3.17	0.67
SD	0.024	0.02	0.02	0.04	0.015	0.24	0.26	0.04
VC	0.740	0.12	0.14	0.10	0.433	0.10	0.08	0.06

V_f, V_c ($\mu m^3/\mu m^2$) are the volume concentrations; R_{eff} (f), R_{eff} (c) (μm) are the effective radii; R_f, R_c (μm) are the volume mean radii and; σ_f and σ_c are the geometric standard deviations; all parameters for fine- and coarse-mode particles, respectively.

such as temperature and relative humidity. The VSDs in the coarse-mode are higher in winter and lower in the summer season, which is attributed to hygroscopic growth of ambient particles (Singh et al., 2004; Tirpathi et al., 2005; Pandithurai et al., 2008; Alam et al., 2012). There observed a noticeable transition from the coarse-mode dominance to the fine-mode at the end of the winter season to the beginning of the spring. This may be due to the onset of the biomass burning in preparation for farming as most of the fine mode particles are anthropogenic in origin (Eck et al., 2005; Tesfaye et al., 2013). The fine-mode aerosol size distribution indicated that the fine peak radius increased from that of the spring (0.15 μm) to the summer (0.2 μm) which denoted an increase in anthropogenic aerosol concentration. Tirpathi et al. (2005) reported an increase in volume concentration in the coarse-mode by 50% during summer season. Pandithurai et al. (2008) found an increase in volume size distribution in summer over Delhi, India. Wang et al. (2011) observed an increase trend in the fine-mode peak radius from summer to winter season for Kanpur AERONET site in India. Alam et al. (2011) also found an increase in volume concentration in the coarse-mode by 40%–70% during the summer season compared to the other seasons over Karachi in Pakistan.

2.4. Single scattering albedo, asymmetry parameter, refractive index

The single scattering albedo (SSA) provides important information regarding scattering and absorption properties of aerosols and is used as a key parameter for estimating ARF. The sign at the top-of-atmosphere (TOA) forcing can change depending on the aerosol SSA (Takemura et al., 2002). It has thus a vital role in understanding the climatic effects of the aerosols. SSA is defined as the ratio between the particle scattering coefficient and total extinction coefficient. The values of SSA strongly depend on the aerosol composition and size distribution (Dubovik et al., 2002). It is zero for pure absorption (*e.g.*, soot) and one for pure scattering (*e.g.*, sulfate). SSA for urban-industrial aerosol as retrieved from worldwide AERONET stations ranging from 0.90 to 0.98 and for biomass burning between 0.88 and 0.94 at lower wavelength (Dubovik et al., 2002; Eck et al., 2003a). SSA was found to be wavelength dependent due to the influence of dust and anthropogenic activities during both the summer and winter seasons. Spectral variations in the SSA differ between dust and urban anthropogenic pollution, with the SSA tending to increase rapidly with increasing wavelength during dust events but to decrease during periods of increased urban pollution (Dubovik et al., 2002).

The seasonal mean spectral variation of SSA over the period of January–December 2012 is shown in Fig. 8a and the vertical bars represent the standard deviation to the mean. It is clear from the figure that the SSA values are lower in winter and higher in summer. The maximum SSAs are found in summer and are 0.976, 0.962, 0.953, and 0.950 at 440, 675, 870 and 1020 nm, respectively. When dust is not the major contributor to the atmospheric optical state, SSA has a selective spectral dependence *i.e.*, SSA decreases with increase in wavelength, which is clearly seen from Fig. 8a and is attributed to the presence of a mixture of aerosols from multiple sources. The SSA being greater than 0.9 for all the wavelengths during the summer suggests the abundance of anthropogenic aerosols of urban-industrial pollution which are absorbing in nature rather than scattering, while the spring time value of SSA between 0.8 and 0.9 suggests dominance of aerosols from biomass burning or forest fires. The SSA during the onset of the spring (November) was a little bit higher than 0.9 at lower wavelength which suggests that the urban aerosol tends to have more input in the aerosol loading when compared to the biomass aerosol. The winter SSA wavelength dependence is similar to that of the spring, while that of autumn is closer to the summer. It can be inferred that the fine mode aerosols prevalent over PTR originates from both urban-industrial and biomass burning sources.

The asymmetry parameter (ASP, *g*) is a simple, single-valued representation of the angular scattering and is a key property controlling the aerosol contribution to forcing. It is defined as the first moment of the particle scattering phase function for clear atmosphere. It is also defined as the intensity-weighted average cosine of the scattering angle and is expressed mathematically as follows:

$$g = \frac{1}{2}\int_0^{\pi} \cos\theta P(\theta)\sin\theta \mathrm{d}\theta \tag{3}$$

where, θ is the angle between the transmitted and the scattered radiation and P(θ) is the phase function (angular distribution of scattered light). The value of g ranges between −1 for entirely backscattered light to +1 for entirely forward scattered light. Like the SSA, the ASP is also a spectral dependent parameter. Fig. 8b shows the spectral variation of ASP for different seasons. There is a consistent decrease in ASP values with increasing wavelengths showing the spectral dependence following a similar trend as AOD. Values of ASP decrease in the visible spectral region and slightly increase in

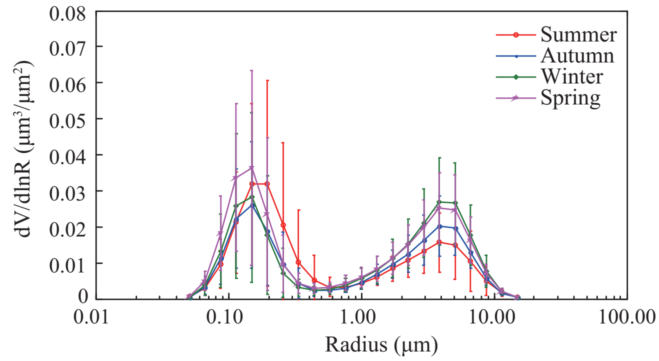

Fig. 7 – Seasonal variations with standard deviations of aerosol volume size distributions derived from sky radiance as a function of particle radiance.

the near infrared region. The average ASP value ranges from 0.71–0.67 to 0.61–0.59 at 440 and 1020 nm, respectively. The greater decrease in ASP was thus observed for the spring (September–November). The results suggest that during this period of the year, the anthropogenic (absorbing) pollutants were relatively in abundance. Similar results were reported by Pandithurai et al. (2008) and Alam et al. (2011, 2012, 2014) over urban areas in India and Pakistan, respectively.

The retrieved real (Re) and imaginary (Im) parts of complex refractive index (RI) for aerosol convey the ability of the scattering and absorption to incoming radiation. The higher real part values correspond to the scattering types and the higher imaginary values correspond to the absorbing type aerosol (Sinyuk et al., 2003). It was reported that the real and imaginary part of urban aerosol has a range of values of 1.40–1.47 and 0.009–0.14, respectively and for biomass burning, the real and imaginary parts have 1.47–1.52 and 0.009–0.02, respectively from four known regions of the world (Dubovik et al., 2002) except, for Moldova where, the imaginary refractive index is 0.0005 for all the wavelengths (Eck et al., 2003b). Fig. 9a and b shows the seasonal mean of the retrieved real and imaginary parts of the refractive indices at 440, 675, 870 and 1020 nm. For the real part, it ranges from 1.38 to 1.45 and imaginary part ranges between 0.004 and 0.024 at 440 nm with weak wavelength dependence. In the case of summer season, no significant wavelength dependence (almost flat) is observed due to the increased anthropogenic pollution over the region. In our investigation, the real (imaginary) part of refractive indices ranges between 1.44 and 1.46 (0.017–0.016) in the spring, from 1.40 to 1.39 (0.004–0.0043) in the summer, from 1.45 to 1.50 (0.023–0.015) in the winter and in the autumn it varies between 1.38 and 1.40 (0.007–0.005). The real values over PTR were highest in the winter season and lowest in the summer. The high values in winter were due to a mixture of aerosols from different sources in the study region. Our results are consistent with those obtained by Alam et al. (2012) over Karachi, Pakistan.

2.5. *Aerosol radiative forcing and efficiency: Model vs. observations*

The aerosol radiative forcing (ARF or RF) at the top-of-atmosphere (TOA) and at the bottom-of-atmosphere/surface (BOA) is defined as the net change in radiative flux (down minus up) in W/m^2 with (F_N) and without (F^o_N) aerosol brought about by instantaneous change of aerosol content in the

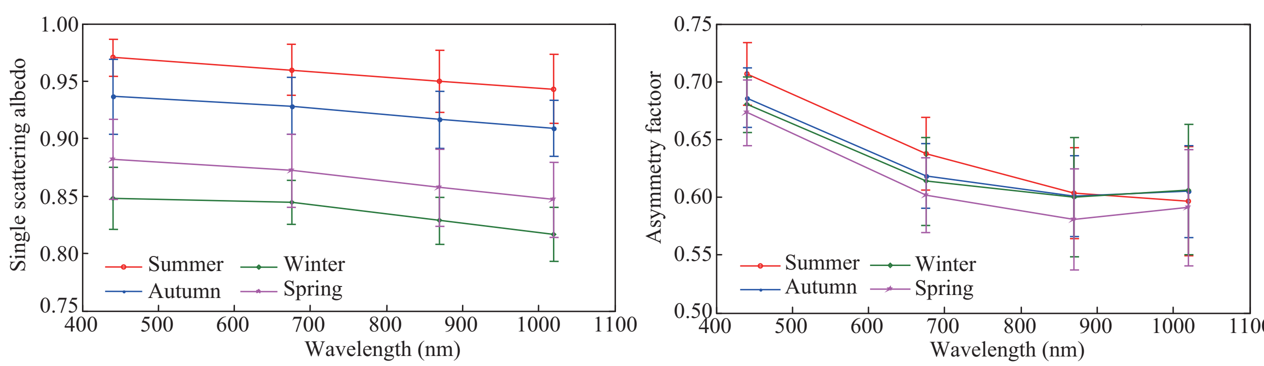

Fig. 8 – Spectral variation of single scattering albedo (SSA) (a) and asymmetry parameter (b) for four seasons.

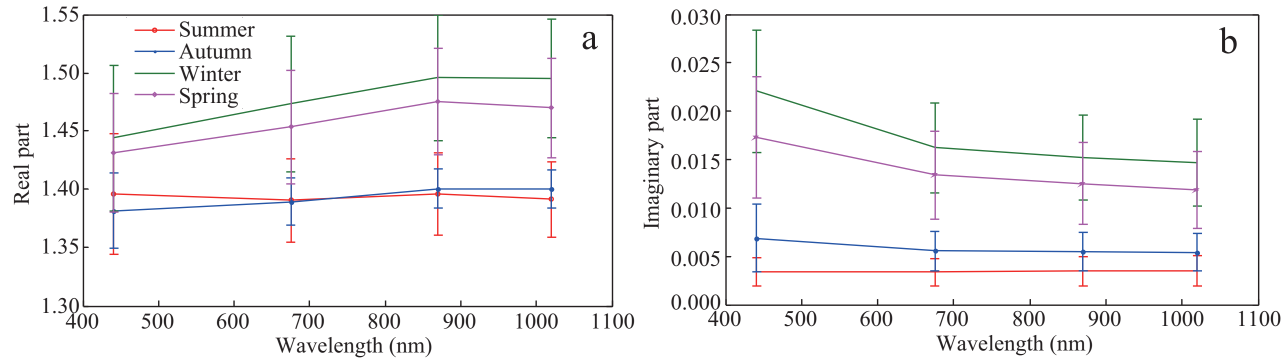

Fig. 9 – Spectral variation of the complex refractive index (a) and real part (b) imaginary part at 440 nm, 675 nm, 870 nm and 1020 nm for four seasons.

atmosphere. The radiative forcing at BOA is given by:

$$RF_{BOA} = F_{N,BOA} - F^{o}_{N,BOA}. \quad (4)$$

The radiative forcing for the atmosphere (RF_{ATM}) can be derived from the radiative forcings at TOA and BOA:

$$RF_{ATM} = RF_{TOA} - RF_{BOA}. \quad (5)$$

Basically, RF_{BOA} represents the combined effects of scattering and absorption of solar radiation by air suspended particles on the net flux at the surface, RF_{TOA} accounts for the reflection of solar radiation to space by aerosols, and RF_{ATM} for the absorption of solar radiation within the atmosphere due to absorbing particles (*e.g.*, Mallet et al., 2006). With the sign criteria adopted here, negative values of RF correspond to an aerosol cooling effect and positive values to warming. In our present study, we made use of TOA and BOA forcing values obtained directly from AERONET inversion product and also computed using Santa Barbara DISORT Atmospheric Radiative Transfer (SBDART) model (Ricchiazzi et al., 1998) to estimate atmospheric radiative forcing.

AERONET Inversion product comes with TOA and BOA representing the upward and downward fluxes measured by the Sunphotometer. These fluxes are integrated over the 0.3–4.0 μm range including their values in the absence of aerosols. All the broadband fluxes are simulated using an interpolation and extrapolation of the real and imaginary parts of the complex refractive index retrieved at AERONET wavelengths. The spectral dependence of surface reflectance is interpolated/extrapolated from surface albedo values assumed in the retrieval of the wavelengths of sun/sky radiometer. The aerosol radiative forcing efficiency (*FE*) which provides the actual or total radiative effects of atmospheric aerosol is defined as the rate at which the atmosphere is forced per unit of aerosol optical depth taken at a reference wavelength (500 nm, in this work) which can be calculated at both BOA (and TOA) with:

$$FE_{BOA} = RF_{BOA}/AOD_{500}. \quad (6)$$

Table 2 – Comparison of monthly mean AERONET derived and SBDART calculated aerosol radiative forcing (ARF) and forcing efficiencies at the surface (BOA) and top of the atmosphere (TOA) along with the heating rate (HR).

Month	AERONET derived ARF				SBDART calculated ARF				
	Radiative forcing (W/m^2)		Forcing efficiency (W/m^2)		Radiative forcing (W/m^2)		Forcing efficiency (W/m^2)		Heating rate (K/day)
	TOA	BOA	TOA	BOA	TOA	BOA	TOA	BOA	
Jan-12	−12.92	−22.74	−91.17	−172.58	−7.48	−17.1	−44.35	−101.41	0.27
Feb-12	−23.04	−40.76	−82.68	−159.51	−18.31	−35.44	−53.85	−104.27	0.48
Mar-12	−11.05	−22.87	−91.05	−189.59	−7.35	−18.14	−48.91	−120.74	0.30
Apr-12	−10.65	−23.07	−84.12	−196.40	−8.43	−19.35	−56.72	−130.23	0.31
May-12	−12.28	−31.24	−78.62	−210.39	−10.68	−24.20	−57.90	−131.22	0.37
Jun-12	−6.60	−22.77	−65.63	−262.34	−3.49	−20.32	−32.78	−190.56	0.47
Jul-12	−10.07	−35.78	−66.31	−247.99	−8.65	−27.28	−49.99	−157.62	0.52
Aug-12	−11.39	−49.04	−53.41	−244.97	−9.70	−37.17	−39.12	−149.93	0.77
Sep-12	−11.91	−41.99	−62.51	−231.73	−9.63	−38.60	−42.23	−169.31	0.81
Oct-12	−12.01	−36.14	−70.10	−232.60	−7.41	−30.75	−36.28	−150.59	0.65
Nov-12	−12.70	−31.05	−82.09	−207.16	−7.14	−24.35	−38.64	−131.78	0.48
Dec-12	−11.24	−21.19	−90.49	−173.56	−7.13	−15.65	−46.42	−101.89	0.23

The two factors, radiative forcing and radiative forcing efficiency are not independent of Solar Zenith Angle (SZA) and the forcing efficiency for different types of aerosol is calculated using similar ranges of SZA values (El-Metwally et al., 2011).

Recently, many earlier researchers have discussed the working principles of this model (Prasad et al., 2007; Alam et al., 2011, 2012; Srivastava et al., 2011, 2012 and references therein). A brief explanation therefore is provided in this paper. In modeling of aerosol effects on atmospheric radiation, the following aerosol optical properties like AOD, SSA, ASP were obtained from PTR AERONET site. Besides these, other input parameters include model atmospheric profile and surface albedo values were obtained from Moderate resolution Imaging Spectroradiometer (MODIS) satellite data over PTR. Another such parameter is the SZA, which is calculated by using a small code in the SBDART model specifying a particular date, time, latitude, and longitude (Alam et al., 2012).

A very good correlation was observed between AERONET derived forcing values and SBDART computed forcing magnitude (figure not shown). The correlation coefficient for the above two is 0.84 in the case of TOA, and the surface forcing is about 0.94 while the ARF stands at 0.88. The monthly variations are listed in Table 2 which shows that both AERONET and SBDART have negative TOA values for all the months which are an indication of net cooling. The TOA value ranges from −6.6 W/m^2 in June to −23 W/m^2 in February, with an annual mean value of −12.2 W/m^2 for AERONET whereas, the SBDART model computed value ranges between −3.5 W/m^2 in June to −18.3 W/m^2 in February and an annual mean of −8.8 W/m^2. The surface forcing for AERONET ranges from −21.2 W/m^2 in December to −49 W/m^2 in August with an annual mean of −31.6 W/m^2. While for SBDART, it is in the range from −15.6 W/m^2 in December to −37.2 W/m^2 in August and annual mean of −25.7 W/m^2. The resultant atmospheric forcing (ARF) values derived from AERONET range from 9.8 W/m^2 in January to 37.6 W/m^2 in August having all values positive throughout the year indicating a warming effect with an annual mean of +19.4 W/m^2 and for SBDART, it ranges from 8.5 W/m^2 in December to 29 W/m^2 in September and annual mean of +16.9 W/m^2. Although the AOD was highest in February, the results show that there is significant heating of the atmosphere between August and September/October (see Table 2) which corresponds to increase in temperatures and production of carbon from biomass burning during the spring months.

The forcing efficiency at the TOA (BOA) from AERONET ranges from −53.4 W/m^2 (−159.5 W/m^2) in August (February) to −91 W/m^2 (−262 W/m^2) in January (June) with an annual mean of −76.5 W/m^2 (−210.7 W/m^2). In the case of SBDART, the TOA (BOA) values range from −32.8 (−101.4) W/m^2 in June (January) to −57.9 W/m^2 (−190.5 W/m^2) in May (June) with an annual mean of −45.6 W/m^2 (−136.6 W/m^2) (see Table 2). An important feature of these results is that the surface level relative forcing was not governed primarily by the AOD values as reflected from the results obtained from AERONET and that calculated using SBDART unlike the work reported by Srivastava et al. (2011), where the surface forcing at Kanpur and Gandhi College (two AERONET sites in India) was primarily governed by the magnitude of AOD values. A similar comparison of RF values at BOA, TOA and ATM for different stations of urban environment over the globe is presented in Table 3.

The net atmospheric forcing given by Eq. (5) represents the amount of radiative flux absorbed by the atmosphere due to the presence of aerosols. This energy is converted into heat inside the layers containing the absorbing particles, which results in an increase of their temperature and alters regional climate (*e.g.*, Ramanathan et al., 2007; Pilewskie, 2007). Using the basic laws of thermodynamics, the derivation of the temporal rate of this increase (atmospheric heating rate) is straightforward (Liou, 2002):

$$\frac{\partial \mathrm{T}}{\partial \mathrm{t}} = \frac{\mathrm{g}}{C_\mathrm{p}}\frac{\Delta F}{\Delta P}. \tag{7}$$

In this equation, the left hand term represents the atmospheric heating rate (HR) in K/sec where T is the temperature in Kelvin (K), t is the time in seconds (sec), g is the gravitational acceleration (9.8 m/sec^2), C_p is the specific heat capacity of dry air at constant pressure (1006 J/kg/K) and ΔP is the height of the column containing the aerosol particles expressed as the difference of atmospheric pressure between its bottom and its top. The radiative heating was therefore

Table 3 – Comparison of aerosol radiative forcing (ARF) at the surface (BOA) and top of the atmosphere (TOA) along with the heating rate (HR) derived in the present study with that of the previous studies reported over some urban stations.

Site	Study period	BOA (W/m^2)	TOA (W/m^2)	ARF (W/m^2)	HR (K/day)	Reference
Pretoria	Jan–Dec, 2012	−15 to −39	−7 to −18	+8 to +29	0.2 to 0.8	Present study
Delhi	2007	−69 to −78	–	+78 to +98	–	Srivastava et al. (2012)
Kanpur	2001–2010	−42 to −57	−12 to −18	+25 to +44	0.8 to 1.2	Kaskaoutis et al. (2013)
Hyderabad	2008–2009	−65 to −80	−17 to −23	+50 to +70	1.6 to 2.0	Sinha et al. (2013)
Bangalore	Nov 2004–May 2005	−20 to −40	+2 to +5	+20 to +45	–	Satheesh et al. (2010)
Ahmedabad	2006–2008	−31 to −41	−4 to −12	+23 to +36	0.4 to 0.6	Ramachandran and Kedia (2012)
Pune	Oct 2004–May 2005	−33 to −47	−0.5 to +0.6	+33 to +48	–	Panicker et al. (2010)
Gosan	2001–2008	−27.5	−15.8	+10 to +16	1.5 to 3.0	Kim et al. (2010)
Cairo	Oct 2004–Mar 2006	−46 to −81	−15 to −25	+29 to +45	1.3 to 2.3	El-Metwally et al. (2011)
Lahore	Mar 2009–Nov 2010	−93 to −98	−19 to −28	+70 to +74	–	Alam et al. (2014)
Spain	2003–2011	−6 to −29	−1.5 to −3.9	–	–	Esteve et al. (2014)
Nanjing	2011–2012	–	−6.9 to +4.5	–	–	Zhuang et al. (2014)

generally higher from August to October than the other months with values 0.77, 0.81 and 0.65 K/day (Table 2). The annual mean heating rate being 0.47 K/day observed for the entire study period over PTR. In terms of seasonal effect, aerosol contributes 0.33 K/day both in summer and autumn, 0.58 K/day in winter and 0.65 K/day in spring which is almost twice that of summer and autumn.

3. Summary and conclusions

Analysis of spectral aerosol optical properties and inversion retrievals of column integrated aerosol microphysical properties over the entire annual cycle was performed over an urban city (PTR) in South Africa. One year data (January–December, 2012) has been used in the present study which is obtained from the AERONET website measured using Cimel Sunphotometer to analyze the aerosol loading in association with local meteorology and estimated the atmospheric radiative forcing from SBDART model. Continuous monitoring of aerosol properties is necessary in order to assess more accurately and in characterizing the annual cycle, since only one year of data has been used in the present study. The aerosol optical depth (AOD) showed two maxima occurring in February and August with magnitude of 0.36 and 0.25, respectively, while the minimum was noticed in April/June (0.12). The seasonal average showed the highest in the summer of 0.24 and the lowest of 0.16 during the autumn. In most of the Southern African countries, the spring season is known to have the highest AOD due to seasonal changes in anthropogenic emission, meteorological conditions or specific topography of the study region.

The monthly mean Angstrom exponent $\alpha_{440-870}$ has a peak value of 1.70 in the month of January and the lowest in June of 1.38, whereas in terms of seasonal variation, the summer has its highest at 1.67 and the lowest in winter with a magnitude of 1.41. For $AOD_{500} < 0.4$, a wide range of α exist between 0.8 and 2.0 and the correlation coefficient between AOD_{500} and $\alpha_{440-870}$ is 0.52. CWV ranges between 0.3 and 2.5 with a correlation coefficient of 0.41 with AOD_{500}, while α showed a positive correlation of 0.55 with CWV.

Optical inversions of sky radiance indicate that the variation in aerosol volume size distribution (VSD) showed a bimodal lognormal distribution with dominance in aerosol fine-mode. The SSA was generally greater than 0.9 for all wavelengths during the summer, while in the spring time, SSA values fall between 0.8 and 0.9. The asymmetry parameter (ASP) ranges between 0.59 and 0.70 during most of the year suggesting that the atmosphere was not generally clean. The average atmospheric forcing computed from SBDART model during the study period was 16.91 ± 6.8 W/m^2, indicating significant heating of the atmosphere with an annual mean heating rate of 0.47 K/day over Pretoria.

Acknowledgments

The authors sincerely thank UKZN, South Africa and NUIST, China for providing enabling environment to carry out the present work. The present work is also supported through Africa Laser Centre (Pretoria) collaborative project and funded NRF bi-lateral project (Grand UID: 78682). One of the authors (AJA) acknowledges the coordinator mastering the Master's program, Fortune Shonhiwa for organizing a writing retreat as the manuscript was prepared. The author KRK thanks Prof. Yin Yan, Dr. Yiwei Diao, Dr. Na Kang and Dr. Xingna Yu for their kind and meticulous help to get settle down at NUIST, China. Authors are grateful to the PIs of AERONET site at Pretoria_CSIR_DPSS and his assistants for the upkeep of the instrument and availability of the online data. We also acknowledge the South Africa Weather Service (SAWS) for utilizing the meteorological data used in this publication. Thanks are also due to Prof. Hongxiao Tang, Editor-in-Chief of the journal and the two anonymous reviewers for their critical comments and insightful suggestions which helped to improve the clarity and scientific content of the original paper.

REFERENCES

Alam, K., Trautmann, T., Blaschke, T., 2011. Aerosol optical properties and radiative forcing over mega-city Karachi. Atmos. Res. 101 (3), 773–782.

Alam, K., Trautmann, T., Blaschke, T., Majid, H., 2012. Aerosol optical and radiative properties during summer and winter season over Lahore and Karachi. Atmos. Environ. 50, 234–245.

Alam, K., Sahar, N., Iqbal, Y., 2014. Aerosol characteristics and radiative forcing during pre-monsoon and post-monsoon seasons in an urban environment. Aerosol Air Qual. Res. 14 (1), 99–107.

Ångström, A., 1964. The parameters of atmospheric turbidity. Tellus 16 (1), 64–75.

Bi, J.R., Huang, J.P., Fu, Q., Wang, X., Shi, J.S., Zhang, W., et al., 2011. Toward characterization of the aerosol optical properties over Loess Plateau of Northwestern China. J. Quant. Spectrosc. Radiat. Transf. 112 (2), 346–360.

Cattrall, C., Reagan, J.A., Thome, K., Dubovik, O., 2005. Variability of aerosol and spectral lidar and backscatter and extinction ratios of key aerosol types derived from selected Aerosol Robotic Network locations. J. Geophys. Res. 110 (D10). http://dx.doi.org/10.1029/2004JD005124.

Chung, C.E., Ramanathan, V., Kim, D., Podgorny, I.A., 2005. Global anthropogenic aerosol direct forcing derived from satellite and ground-based observations. J. Geophys. Res. 110, D24207. http://dx.doi.org/10.1029/2005JD006356.

Devara, P.C.S., Saha, S.K., Raj, P.E., Sonbawne, S.M., Dani, K.K., Tiwari, Y.K., et al., 2005. A four-year climatology of total column tropical urban aerosols, ozone and water vapor distributions over Pune, India. Aerosol Air Qual. Res. 5 (1), 103–114.

Draxler, R.R., Hess, G.D., 1998. An overview of the HYSPLIT_4 modelling system for trajectories, dispersion and deposition. Aust. Meteorol. Mag. 47 (4), 295–308.

Draxler, R.R., Rolph, G.D., 2003. HYSPLIT Model Access via NOAA ARL READY Website (http://www.arl.noaa,gov/ready/hysplit4.html). NOAA Air Resources Laboratory, Silver Spring, MD.

Dubovik, O., King, M.D., 2000. A flexible inversion algorithm for retrieval of aerosol optical properties from Sun and sky radiance measurements. J. Geophys. Res. 105 (D16), 20673–20696.

Dubovik, O., Smirnov, A., Holben, B.N., King, M.D., Kaufman, Y.J., Eck, T.F., et al., 2000. Accuracy assessments of aerosol optical properties retrieved from Aerosol Robotic Network (AERONET)

Sun and Sky radiance measurements. J. Geophys. Res. 105 (D8), 9791–9806.
Dubovik, O., Holben, B.N., Eck, T.F., Smirnov, A., Kaufman, Y.J., King, M.D., et al., 2002. Variability of absorption and optical properties of key aerosol types observed in worldwide location. J. Atmos. Sci. 59 (3), 590–608.
Dubovik, O., Sinyuk, A., Lapyonok, T., Holben, B.N., Mishchenko, M., Yang, P., et al., 2006. Application of light scattering by spheroids accounting for particle non-sphericity in remote sensing of desert dust. J. Geophys. Res. 111, D11208. http://dx.doi.org/10.1029/2005JD006619.
Eck, T.F., Holben, B.N., Reid, J.S., Dubovik, O., Smirnov, A., O'Neill, N.T., et al., 1999. Wavelength dependence of the optical depth of biomass burning, urban and desert dust aerosols. J. Geophys. Res. 104 (D24), 31333–31349.
Eck, T.F., Holben, B.N., Reid, J.S., O'Neil, N.T., Schafer, J.S., Dubovik, O., et al., 2003a. High aerosol optical depth biomass burning events: a comparison of optical properties for different source regions. Geophys. Res. Lett. 30 (20), 2035. http://dx.doi.org/10.1029/2003GL017861.
Eck, T.F., Holben, B.N., Ward, D.E., Mukelabai, M.M., Dubovik, O., Smirnov, A., et al., 2003b. Variability of biomass burning aerosol optical characteristics in southern Africa during the SAFARI 2000 dry season campaign and a comparison of single scattering albedo estimates from radiometric measurements. J. Geophys. Res. 108 (D13), 8477. http://dx.doi.org/10.1029/2002JD002321.
Eck, T.F., Holben, B.N., Dubovik, O., Smirnov, A., Goloub, P., Chen, H.B., et al., 2005. Columnar aerosol optical properties at AERONET sites in central Eastern Asia and aerosol transport to the tropical mid-pacific. J. Geophys. Res. 110 (D6), D06202. http://dx.doi.org/10.1029/2004JD005274.
El-Metwally, M., Alfaro, S.C., Wahab, M.M.A., Favez, O., Mohamed, Z., Chatenet, B., 2011. Aerosol properties and associated radiative effects over Cairo (Egypt). Atmos. Res. 99 (2), 263–276.
Esteve, A.R., Estelles, V., Utrilla, M.P., Lozano, J.A.M., 2014. Analysis of the aerosol radiative forcing over a Mediterranean urban coastal site. Atmos. Res. 137, 195–204.
Holben, B.N., Eck, T.F., Slutsker, I., Tanre, D., Buis, J.P., Setzer, A., et al., 1998. AERONET — a federated instrument network and data archive for aerosol characterization. Remote Sens. Environ. 66 (1), 1–16.
Intergovernmental Panel on Climate Change (IPCC), 2001. Climate Change 2001: The Scientific Basis. In: Houghton, J.T., Ding, Y., Griggs, D.J., Noguer, M., van der Linden, P.J., Dai, X., et al. (Eds.), Contribution of Working Group I to the Third Assessment Report of the Intergovernmental Panel on Climate Change. Cambridge University Press, New York.
Intergovernmental Panel on Climate Change (IPCC), 2007. Climate change 2007: the physical science basis. Contribution of Working Group I to the Fourth Assessment Report of the Intergovernmental Panel on Climate Change: Chapter 2, p. 129.
Kahn, R.A., Gaitley, B.J., Garay, M.J., Diner, D.J., Eck, T.F., Smirnov, A., et al., 2010. Multiangle Imaging Spectroradiometer global aerosol product assessment by comparison with the Aerosol Robotic Network. J. Geophys. Res. 115 (D231), D23209. http://dx.doi.org/10.1029/2010JD014601.
Kaskaoutis, D.G., Sinha, P.R., Vinoj, V., Kosmopoulos, P.G., Tripathi, S.N., Misra, A., et al., 2013. Aerosol properties and radiative forcing over Kanpur during severe aerosol loading conditions. Atmos. Environ. 79, 7–19.
Kaufman, Y.J., Tanre, D., Boucher, O., 2002. A satellite view of aerosols in climate system. Nature 419 (6903), 215–223.
Kiehl, J.T., Briegle, B.P., 1993. The relative roles of sulfate aerosols and greenhouse gases in climate forcing. Science 260 (5106), 311–314.
Kim, S.W., Choi, I.J., Yoon, S.C., 2010. A multi-year analysis of clear-sky aerosol optical properties and direct radiative forcing at Gosan, Korea (2001–2008). Atmos. Res. 95 (2–3), 279–287.
Kumar, K.R., Narasimhulu, K., Reddy, R.R., Gopal, K.R., Reddy, L.S. S., Balakrishnaiah, G., et al., 2009. Temporal and spectral characteristics of aerosol optical depths in a semi-arid region of Southern India. Sci. Total Environ. 407 (8), 2673–2688.
Kumar, K.R., Sivakumar, V., Reddy, R.R., Gopal, K.R., Adesina, A.J., 2013a. Inferring wavelength dependence of AOD and Ångström exponent over a sub-tropical station in South Africa using AERONET data: Influence of meteorology, long-range transport and curvature effect. Sci. Total Environ. 461–462, 397–408.
Kumar, K.R., Adesina, A.J., Sivakumar, V., 2013b. Aerosol radiative forcing from spectral solar attenuation measurements due to aerosol loading using AERONET over Pretoria in South Africa. Proceedings of 2013 IEEE Annual International Conference on Emerging Research Areas: International Conference on Microelectronics, Communications and Renewable Energy., IEEE, Kanjirappally, Kerala, India., 1–4, June 4–6.
Levy, R.C., Remer, L.A., Dubovik, O., 2007. Global aerosol optical properties and application to moderate resolution imaging spectroradiometer: aerosol retrieval over land. J. Geophys. Res. 112, D13210. http://dx.doi.org/10.1029/2006JD007815.
Liou, K.N., 2002. An Introduction to Atmospheric Radiation. Elsevier, New York, p. 583.
Lohmann, U., Rotstayn, L., Storelvmo, T., Jones, A., Menon, S., Quaas, J., et al., 2010. Total aerosol effect: radiative forcing or radiative flux perturbation? Atmos. Chem. Phys. 10, 3235–3246.
Lyamani, H., Olmo, F.J., Alcantara, A., Alados-Arboledas, L., 2006. Atmospheric aerosols during the 2003 heat wave in south-eastern Spain I: spectral optical depth. Atmos. Environ. 40 (33), 6453–6464.
Mallet, M., Pont, V., Liousse, C., Roger, J.C., Dubuisson, P., 2006. Simulation of aerosol radiative properties with the ORISAM-RAD model during a pollution event (ESCOMPTE 2001). Atmos. Environ. 40 (40), 7696–7705.
More, S., Kumar, P.P., Gupta, P., Devara, P.C.S., Aher, G.R., 2013. Comparison of aerosol products retrieved from AERONET, MICROTOPS, and MODIS over a tropical urban city, Pune, India. Aerosol Air Qual. Res. 13 (1), 107–121.
Pandithurai, G., Dipu, S., Dani, K.K., Tiwari, S., Bisht, D.S., Devara, P.C.S., et al., 2008. Aerosol radiative forcing during dust events over New Delhi, India. J. Geophys. Res. 113, D13209. http://dx.doi.org/10.1029/2008JD009804.
Panicker, A.S., Pandithurai, G., Safai, P.D., Dipu, S., Lee, D.I., 2010. On the contribution of black carbon to the composite aerosol radiative forcing over an urban environment. Atmos. Environ. 44 (25), 3066–3070.
Pilewskie, P., 2007. Climate change: aerosols heat up. Nature 448 (7153), 541–542.
Prasad, A.K., Singh, S., Chauhan, S., Srivastava, M.K., Singh, R.P., Singh, R., 2007. Aerosol radiative forcing over the Indo-Gangetic plains during major dust storms. Atmos. Environ. 41 (29), 6289–6301.
Queface, A.J., Piketh, S.J., Eck, T.F., Tsay, S.C., Mavume, A.F., 2011. Climatology of aerosol optical properties in Southern Africa. Atmos. Environ. 45 (17), 2910–2921.
Rajeev, K., Ramanathan, V., Meywerk, J., 2000. Regional aerosol distribution and its long-range transport over the Indian Ocean. J. Geophys. Res. 105 (D2), 2029–2043. http://dx.doi.org/10.1029/1999JD900414.
Ramachandran, S., Kedia, S., 2012. Radiative effects of aerosols over Indo-Gangetic plain: environmental (urban vs. rural) and seasonal variations. Environ. Sci. Pollut. Res. 19 (6), 2159–2171.
Ramanathan, V., Carmichael, G., 2008. Global and regional climate changes due to black carbon. Nat. Geosci. 1 (4), 221–227.
Ramanathan, V., Ramana, M.V., Roberts, G., Kim, D., Corrigan, C.E., Chung, C.E., Winker, D., et al., 2007. Warming trends in Asia

amplified by brown cloud solar absorption. Nature 448 (7253), 575–578.
Ricchiazzi, P., Yang, S., Gautier, C., Sowle, D., 1998. SBDART: a research and teaching software tool for plane-parallel radiative transfer in the Earth's atmosphere. Bull. Am. Meteorol. Soc. 79 (10), 2101–2114.
Satheesh, S.K., Vinoj, V., Moorthy, K.K., 2010. Radiative effects of aerosols at an urban location in southern India: observations versus model. Atmos. Environ. 44 (39), 5295–5304.
Singh, R.P., Dey, S., Tripathi, S.N., Tare, V., Holben, B.N., 2004. Variability of aerosol parameters over Kanpur city, northern India. J. Geophys. Res. 109 (D23). http://dx.doi.org/10.1029/2004JD004966.
Sinha, P.R., Dumka, U.C., Manchanda, R.K., Kaskaoutis, D.G., Sreenivasan, S., Moorthy, K.K., et al., 2013. Contrasting aerosol characteristics and radiative forcing over Hyderabad, India due to seasonal mesoscale and synoptic-scale processes. Q. J. R. Meteorol. Soc. 139 (671), 434–450.
Sinyuk, A., Torres, O., Dubovik, O., 2003. Combined use of satellite and surface observations to infer imaginary part of the refractive index of Saharan dust. Geophys. Res. Lett. 30 (2), L1081. http://dx.doi.org/10.1029/2002GL016189.
Smirnov, A., Holben, B.N., Dubovik, O., O'Neill, N.T., Eck, T.F., Westphal, D.L., et al., 2002. Atmospheric aerosol optical properties in the Persian Gulf. J. Atmos. Sci. 59 (3), 620–634.
Srivastava, A.K., Tiwari, S., Devara, P.C.S., Bisht, D.S., Srivastava, M.K., Tripathi, S.N., et al., 2011. Pre-monsoon aerosol characteristics over the Indo-Gangetic Basin: implications to climatic impact. Ann. Geophys. 29 (4), 789–804.
Srivastava, A.K., Singh, S., Tiwari, S., Bisht, D.S., 2012. Contribution of anthropogenic aerosols in direct radiative forcing and atmospheric heating rate over Delhi in the Indo-Gangetic Basin. Environ. Sci. Pollut. Res. 19 (4), 1144–1158.
Sumit Kumar, S., Devara, P.C.S., Dani, K.K., Sonbawane, S.M., Saha, S.K., 2011. Sun–sky radiometer-derived column-integrated aerosol optical and microphysical properties over a tropical urban station during 2004–2009. J. Geophys. Res. 116, D10201. http://dx.doi.org/10.1029/2010JD014944.
Takemura, T., Nakajima, T., Dubovik, O., Holben, B.N., Kinne, S., 2002. Single-scattering albedo and radiative forcing of various aerosol species with a global three-dimension model. J. Clim. 15 (4), 333–352.
Tesfaye, M., Sivakumar, V., Botai, J., Tsidu, G.M., 2011. Aerosol climatology over South Africa based on 10 years of Multangle Imaging Spectroradiometer (MISR) data. J. Geophys. Res. 116, D20216. http://dx.doi.org/10.1029/2011JD016023.
Tesfaye, M., Botai, J., Sivakumar, V., Tsidu, G.M., 2013. Evaluation of regional climatic model simulated aerosol optical properties over South Africa using ground-based and satellite observations. ISRN Atmos. Sci. 1–17 http://dx.doi.org/10.1155/2013/237483 (Article ID: 237483).
Tirpathi, S.N., Dey, S., Chandel, A., Srivastava, S., Singh, R.P., Holben, B.N., 2005. Comparison of MODIS and AERONET derived aerosol optical depth over the Ganga Basin, India. Ann. Geophys. 23 (4), 1093–1101.
Wang, S.P., Fang, L., Gu, X.F., Yu, T., Geo, J., 2011. Comparison of aerosol optical properties from Beijing and Kanpur. Atmos. Environ. 45 (39), 7406–7414.
Yoon, S.C., Won, J.G., Omar, A.H., Kim, S.W., Sohn, B.J., 2005. Estimation of the radiative forcing by key aerosol types in worldwide locations using a column model and the AERONET data. Atmos. Environ. 39 (35), 6620–6630.
Yu, X., Zhu, B., Fan, S., Yin, Y., Bu, X., 2009. Ground-based observation of aerosol optical properties in Lanzhou, China. J. Environ. Sci. 21 (11), 1519–1524.
Zhuang, B.L., Wang, T.J., Li, S., Liu, J., Talbot, R., Mao, H.T., et al., 2014. Optical properties and radiative forcing of urban aerosols in Nanjing, China. Atmos. Environ. 83, 43–52.

JOURNAL OF ENVIRONMENTAL SCIENCES

环境科学学报(英文版)

(http://www.jesc.ac.cn)

Aims and scope

Journal of Environmental Sciences is an international academic journal supervised by Research Center for Eco-Environmental Sciences, Chinese Academy of Sciences. The journal publishes original, peer-reviewed innovative research and valuable findings in environmental sciences. The types of articles published are research article, critical review, rapid communications, and special issues.

The scope of the journal embraces the treatment processes for natural groundwater, municipal, agricultural and industrial water and wastewaters; physical and chemical methods for limitation of pollutants emission into the atmospheric environment; chemical and biological and phytoremediation of contaminated soil; fate and transport of pollutants in environments; toxicological effects of terrorist chemical release on the natural environment and human health; development of environmental catalysts and materials.

For subscription to electronic edition

Elsevier is responsible for subscription of the journal. Please subscribe to the journal via http://www.elsevier.com/locate/jes.

For subscription to print edition

China: Please contact the customer service, Science Press, 16 Donghuangchenggen North Street, Beijing 100717, China. Tel: +86-10-64017032; E-mail: journal@mail.sciencep.com, or the local post office throughout China (domestic postcode: 2-580).

Outside China: Please order the journal from the Elsevier Customer Service Department at the Regional Sales Office nearest you.

Submission declaration

Submission of an article implies that the work described has not been published previously (except in the form of an abstract or as part of a published lecture or academic thesis), that it is not under consideration for publication elsewhere. The submission should be approved by all authors and tacitly or explicitly by the responsible authorities where the work was carried out. If the manuscript accepted, it will not be published elsewhere in the same form, in English or in any other language, including electronically without the written consent of the copyright-holder.

Submission declaration

Submission of the work described has not been published previously (except in the form of an abstract or as part of a published lecture or academic thesis), that it is not under consideration for publication elsewhere. The publication should be approved by all authors and tacitly or explicitly by the responsible authorities where the work was carried out. If the manuscript accepted, it will not be published elsewhere in the same form, in English or in any other language, including electronically without the written consent of the copyright-holder.

Editorial

Authors should submit manuscript online at http://www.jesc.ac.cn. In case of queries, please contact editorial office, Tel: +86-10-62920553, E-mail: jesc@263.net, jesc@rcees.ac.cn. Instruction to authors is available at http://www.jesc.ac.cn.

Journal of Environmental Sciences (Established in 1989)
Vol. 26 No. 12 2014

Supervised by	Chinese Academy of Sciences	**Published by**	Science Press, Beijing, China
Sponsored by	Research Center for Eco-Environmental		Elsevier Limited, The Netherlands
	Sciences, Chinese Academy of Sciences	**Distributed by**	
Edited by	Editorial Office of Journal of	Domestic	Science Press, 16 Donghuangchenggen
	Environmental Sciences		North Street, Beijing 100717, China
	P. O. Box 2871, Beijing 100085, China		Local Post Offices through China
	Tel: 86-10-62920553; http://www.jesc.ac.cn	Foreign	Elsevier Limited
	E-mail: jesc@263.net, jesc@rcees.ac.cn		http://www.elsevier.com/locate/jes
Editor-in-chief	Hongxiao Tang	**Printed by**	Beijing Beilin Printing House, 100083, China

CN 11-2629/X **Domestic postcode: 2-580** **Domestic price per issue RMB ¥ 110.00**

ISSN 1001-0742

12>

9 771001 074147